International Journal of Nanomedicine

Dovepress
Taylor & Francis Group

Open Access Full Text Article

ORIGINAL RESEARCH

Critical Evaluation of Combined Cu and Fe_3O_4 Nanodots with Gum Arabic Nano-Hybrids Using in-vitro Model: Flow Cytometry and Cell Viability Studies

Sami G Almalki[1], Youssef O Al-Ghamdi[2], Faisal K Algethami[3], Walid M Daoush[3], Bahauddeen M Alrfaei[4,5], Maisa Alanazi[5], Yaser E Alqurashi[6], Mahjoub Jabli[2,7]

[1]Department of Medical Laboratory Sciences, College of Applied Medical Sciences, Majmaah University, Majmaah, 11952, Saudi Arabia; [2]Department of Chemistry, College of Science Al-Zulfi, Majmaah University, Al-Majmaah, 11952, Saudi Arabia; [3]Department of Chemistry, College of Science, Imam Mohammad Ibn Saud Islamic University (IMSIU), Riyadh, 11623, Saudi Arabia; [4]King Saud Bin Abdulaziz University for Health Sciences (KSAU-HS), Ministry of National Guard - Health Affairs (MNGHA), Riyadh, 11426, Saudi Arabia; [5]King Abdullah International Medical Research Center, MNGHA, Riyadh, 11426, Saudi Arabia; [6]Department of Biology, College of Science Al-zulfi, Majmaah University, Al-Majmaah, 11952, Saudi Arabia; [7]Textile Materials and Processes Research Unit, Tunisia National Engineering School of Monastir, University of Monastir, Monastir, 5019, Tunisia

Correspondence: Walid M Daoush, Email wmdaoush@imamu.edu.sa

Background: Previous studies on synthesis and cytotoxicity effect of copper (Cu) and magnetite (Fe_3O_4) nanodots against kidney and lung cancer cells Lines.

Purpose: Investigation of the effects of Cu and Fe_3O_4 nanodots on the reduction in viability of lung cancer (A549) and human embryonic kidney (HEK239T) cells lines.

Methods: Cu and Fe_3O_4 nanodots/Gum Arabic (GA) hybrids were chemically synthesized, characterized, and assessed by MTT and flow cytometry for their cytotoxicity against A549 and HEK239T cells lines.

Results: Novel hybrids of Cu and Fe_3O_4 nanodots were effectively synthesized by chemical deposition method in combination with GA stabilizing agent. The stabilized Cu and Fe_3O_4 nanodots by GA have median particle size of 4.7 nm and 7 nm respectively. Furthermore, the biological activities of Cu nanodots/ GA hybrids showed a strong reduction in viability for both A549 and HEK239T cells at 50 and 100 ng/μL, owing to their small size and high surface-area-to-volume ratio compared to Fe_3O_4 nanoparticles. Pre-apoptosis effect of the Cu nanodots/ GA hybrid on the treated A549 cells were 40% for 0.1 ng/μL, 91.4% for 1 ng/μL, 88% for 50 ng/μL, and 87.7% for 100 ng/μL. However, in the treated human embryonic kidney (HEK293T) cells, the pre-apoptosis was found under different concentrations conditions of 89.9% for 0.1 ng/μL, 94.2% for 1 ng/μL, 76.2% for 50 ng/μL and 70.5% for 100 ng/μL. After treatment of both A549 and HEK293T cells with 100 ng/μL of Cu nanodots/GA hybrid, many cell deaths and reformed nanoparticles crystals were observed.

Conclusion: Cu nanodots/GA hybrid strongly reduce the viability of both A549 and HEK239T cells at 50 and 100 ng/μL. However, Fe_3O_4 nanodots/GA hybrid did not show any significant effect.

Keywords: Cu nanodots, Fe_3O_4 nanodots, Arabic gum, lung cancer, human embryonic kidney cells

Introduction

The unique characteristics and versatile applications of metal and metal oxide nanoparticles have attracted considerable attention owing to their high surface-area-to-volume ratios.[1,2] Indeed, the synthesis and stabilization of nanoparticles with different shapes and sizes using several chemical techniques have been established, including chemical reduction,[3] sono-chemical reduction,[4] microemulsion,[5] photolysis,[6] metal vaporization,[7] radiolysis,[8] the polyol method,[9] and thermal reduction.[10] Among these techniques, chemical reduction is considered a simple, low-cost, and reproducible practical method for fabricating high-purity metallic particles such as Cu nanoparticles. This is an easy method to control the size and shape of

Received: 1 October 2024
Accepted: 23 January 2025
Published: 3 March 2025

the prepared Cu nanoparticles. However, the large-scale production of copper nanoparticles remains difficult owing to their easy oxidation in solution. Hence, stabilization of these nanoparticles against both agglomeration and oxidation is necessary. Many studies have reported the design of stabilized metal nanoparticles in solution, especially in aqueous solutions. For example, Pham et al[11] used argon as a protective gas to fabricate Cu nanoparticles in solutions of different stabilizing or capping agents such as polyvinylpyrrolidone and Cetyltrimethylammonium bromide. Abdulla-Al-Mamun et al[12] reported a method for synthesizing Cu nanoparticles in methyl cyanide using Ar gas. Kobayashi et al[13] used protective nitrogen gas to prepare Cu nanoparticles in citric acid solution. However, inert gases are rare and expensive. Therefore, there is a strong need to prepare metal nanoparticles without using inert gases under atmospheric conditions during the synthesis process. Vaseem et al[14] reduced $CuCl_2$ using hydrazine to obtain Cu nanoparticles in a cetyltrimethylammonium bromide stabilizing solution. Lai et al[15] had reduced $CuSO_4$ with a sodium hypophosphite reducing agent to obtain Cu nanoparticles in a polyvinylpyrrolidone capping solution. However, this process is time consuming and requires heating. Therefore, it is necessary to develop more common techniques for the fabrication of metal nanoparticles.

Recently, Răcuciu et al[16] synthesized iron oxide nanoparticles with a definite particle size distribution through a co-precipitation method in aqueous solutions, using l-aspartic acid as a stabilizing agent. Co-precipitation is a suitable method for producing magnetic nanoparticles (MNPs). The main advantage of this process is that a large quantity of nanoparticles and a high reproducibility can be achieved. However, controlling the particle-size distribution is a limitation of this method. Our previous study by Daoush et al[17] used ethylenediaminetetraacetic acid as a stabilizing agent to permit more nanoparticles to avoid aggregation and decrease the median particle size. Biocompatible super-paramagnetic iron oxide nanoparticles coated with a mixture of ascorbic acid and/or tartaric acid to protect their surface oxidation were developed in a previous study.[18] The saturation magnetization was nearly stable at approximately 62 emu/g after 12 weeks. In another study, iron oxide nanoparticles of different sizes were synthesized using a hydrothermal process. By increasing the particle size, the ratio of magnetite to the maghemite phase increased, reaching a pure magnetite phase with a particle size of 123 ± 44 nm.[19] Researchers have successfully prepared superparamagnetic iron oxide nanoparticles with diameters of almost 7 nm using a co-precipitation method with an oleate coating agent.[20] The crystal size of the nanoparticles was increased by adjusting the hydrothermal conditions such as the reaction temperature and time; hence, nanoparticles with diameters of approximately 11 nm were obtained.[20] In another study, iron oxide nanoparticles were synthesized in air atmosphere using a co-precipitation method.[21] Lowering the iron ion concentration in solution reduced both particle size and crystallinity. The obtained nanoparticles show superparamagnetic behavior at room temperature and the saturation magnetization is increased up to 63.71 emu/g and the particle sizes vary from 7.45 nm to 4.88 nm with the change of iron ion concentration.[21]

The use of natural polymers as stabilizing or capping agents is a promising method for preparing metal nanoparticles by preventing their aggregation in solution during synthesis. Zhang et al[22] prepared copper nanoparticles using gelatin as a capping agent. Gum acacia has also been applied as a natural immobilizing matrix for instant stabilization of freshly prepared AgNPs.[23] The most commercially important species of Gum acacia are the *Acacia Senegal* and *Acacia Seyal which* named after discovering the GA extruded by the trees of *Acacia Senegal* and *Acacia Seyal*, produce GA.[24,25] The most commercially important species of Gum acacia are the *Acacia Senegal* and *Acacia Seyal which* named after discovering the GA extruded by the trees of *Acacia Senegal* and *Acacia Seyal*, produce GA.[24,25] GA is a naturally-occurring, non-toxic, water-loving, extensively-branched polysaccharide obtained from the exudates of Acacia senegal and Acacia seyal trees. Due to its biocompatibility and its ability to stabilize and emulsify, GA has been applied in the field of nanomedicine. Suárez-Cerda et al[26] developed a copper nanoparticle synthesis process through the chemical reduction of an aqueous solution of copper sulfate with ascorbic acid as the reducing agent, using different native cyclodextrins as stabilizing agents. El-Batal et al[27] prepared copper nanoparticles using citrus pectin, chitosan, and sodium alginate, with P. ostreatus as a reducing agent. Prince et al[28] synthesized Cu nanoparticles using L-ascorbic acid as a reducing agent stabilized with GA.[28]

The use of GA as a dispersing and capping agent can prevent nanoparticle aggregation and provide nanoparticles dispersed in solutions for a prolonged period of stability. It has been reported in the literature[29] that the use of an GA capping agent can stabilize nanoparticles such as carbon nanotubes and iron oxide/carbon nanotube nanocomposites in aqueous and polar solvents and electrolytes under the effect of ultrasonic waves with a frequency of 40 kHz. Owing to the biocompatibility of biopolymers, GA-capped metal and metal oxide nanoparticles can be used in medical and

pharmaceutical applications. Herein, our goal is to prepare Cu and Fe_3O_4 nanodots/GA hybrids using a chemical deposition method. The produced nanoparticles were characterized using a series of analytical methods, namely field emission scanning electron microscope (FE-SEM), energy dispersive X-ray (EDX), X ray diffraction (XRD), Fourier transform infrared spectroscopy (FT-IR), high resolution transmission electron microscope (HR-TEM) and high resolution field emission transmission electron microscopy (HRFE-TEM). The magnetic properties were measured using the vibrating sample magnetometer (VSM) method. By dispersing the nanoparticles in an emulsifying agent composed of natural GA and a biocompatible polymer at low cost to handle and enhance the effectiveness of the investigated cells, the process will be ecofriendly and recommend GA as a good emulsifying agent for medical applications as well as a good drug carrier agent for cancer therapy. The applicability of the 3-[4,5-dimethylthiazol-2-yl]-2,5 diphenyl tetrazolium bromide (MTT) assay and (annexin V/propidium iodide) cytometry assay in a typical context for testing the effect of the synthesized Cu nanodots/GA and Fe_3O_4 nanodots/GA hybrids on the reduction in viability of embryonic kidney (HEK293T) and lung cancer cell lines (A549) has also been reported and evaluated.

Materials and Methods

The GA has provided from the Saudi special service laboratory, Riyadh; Saudi Arabia (License no. 172, Catalog. No. 6281103383762) by drying exudates of the trunks and branches of Acacia trees of the family Fabaceae or Leguminosae, from some harvested wild trees.[24,25] The obtained extruded gum used for the combination with Cu and Fe_3O_4 nanodots and the formation of new hybrids by stabilization in an aqueous solution. All reagents used in this study are highly pure grade and used without further purification, namely potassium sodium tartrate, copper sulfate pentahydrate, sodium hydroxide, ferric chloride hexahydrate, ferrous chloride tetrahydrate, and ammonia solution.

The Preparation of Cu and Fe_3O_4 Nanodots/GA Hybrids

Cu nanodots are synthesized by chemical deposition method. Copper sulfate pentahydrate and potassium sodium tartrate are dissolved in aqueous solution and magnetically stirred at 500 rpm and 25°C for 15 min. The pH of the solution is adjusted with sodium hydroxide to 12.5, using a pH meter connected to a glass electrode, followed by the addition of a formaldehyde reducing agent to enhance the chemical reduction of Cu ions to produce Cu nanodots. Subsequently, a 1% freshly prepared aqueous solution of GA at 100°C for 30 min is added to the aqueous solution under continuous stirring for 1 h to obtain a Cu nanodots hybrid combined with GA suspended in the solution. The obtained solution is centrifuged at 3000 rpm to collect the Cu nanodots/GA hybrid for further characterization.

Fe_3O_4 nanodots are synthesized by developing a method based on previous reports with some modifications.[16,17] In the co-precipitation method, the chemical deposition method, ferric chloride hexahydrate solution (4 mmol), and ferrous chloride tetrahydrate solution (2 mmol) were mixed and magnetically stirred at 500 rpm and 60°C. The dropwise addition of the ammonia solution favored the co-precipitation of the Fe_3O_4 nanodots. Subsequently, a freshly prepared aqueous solution containing 1wt. % GA is added to the above mixture under continuous stirring during 1h to get Fe_3O_4 nanodots hybrid by combination with the GA in solution. The prepared solution underwent centrifugation at 3000 rpm for 5 min. to collect the Fe_3O_4 nanodots/GA hybrid for further characterization.

The Electron Microscopy, XRD, FT-IR Spectrum and Magnetic Properties

The morphological characteristics of the nanoparticles are analyzed using FE-SEM of model (JEOL, JSM-7600F) connected to an EDX unit. The powders of the investigated Cu and Fe_3O_4 nanodots are coated with platinum using a vacuum sputter-coater unit to improve their conductivity, and the secondary electron image resolutions are also examined using FE-SEM. The acceleration voltage is set to 20 kV. The different functional groups of the produced Cu nanodots/GA and the Fe_3O_4 nanodots/Arabic gum hybrids are identified by FT-IR spectrum analysis. The crystal structures of the produced Cu and Fe_3O_4 nanodots are determined using XRD (D8 Discover Bruker) with 2 theta range of 10° to 90°. TEM of model (JEOL, JEM-1011) operated at an acceleration voltage of 300 kV and HRFE-TEM of model (JEOL, JEM-2100F) used to investigate the morphology of the Cu and Fe_3O_4 nanodots, as well as their particle size and distribution. The Cu and Fe_3O_4 nanodots are separately dispersed in ethanol under ultrasonic agitation for 10 min and then deposited on a Cu grid. Magnetic properties are measured at room temperature under an applied field of

2 Tesla by VSM of model 7400 Series VSM, Lake Shore Cryotronics, Inc., OH, USA). The measured magnetic properties, including saturation magnetization (M_s), retentivety (M_r), and coercive force (H_c), are computed from the hysteresis loop of the magnetization/field correlation for each sample.

Cell Lines and Culture Conditions

The lung Cancer Cell Lines-A549-(ATCC-CRM-CCL-185) and HEK293T (ATCC-CRL-3216) are purchased from American Type Culture Collection (ATCC). The cells are grown to 70% confluence. The culture medium consisted of Dulbecco's modified Eagle's medium with low glucose (DMEM, #31885, Gibco), 10% fetal bovine serum (FBS, #10091148, Gibco), 1% antibiotic (Gibco, #15140–122), and 1% glutamine (Gibco, #25030-024). All investigated cultured cells are incubating in humidified conditions at 37°C and 5% CO_2.

Cell Viability and MTT Assay

The cells were inoculated into 96-well plates at a density of 5000 cells/well and incubated at 37°C °C overnight. The cells are then starved in 1% FBS for 24 h. After starvation for one day, the cells are separately incubated overnight under exposure to different concentrations of Cu nanodots/Arabic gum and Fe_3O_4 nanodots/GA hybrids. Cell viability is quantified using the CellTiter-Glo Luminescent Cell Viability Assay (Promega # G7570, Madison, Wisconsin, United States) as described previously report of the literature.[30] Fluorescence intensity is measured on a SpectraMax M5 Reader using SoftMax Pro v.7.0.2.

Flow Cytometry and Pre-Apoptosis Assay

According to a previously described protocol reported in the literature,[31] samples containing live dissociated cells are stained for dead cells and pre-apoptosis cells using the annexin V Alexa Fluor antibody and propidium iodide kit (Thermo Fisher Scientific #V13241). The samples analyzed using fluorescence-activated cell sorting (FACS) CANTO II (BD Biosciences). The cells are starved for 24 h and then treated separately with the produced Cu nanodots-Arabic gum and Fe_3O_4 nanodots/GA hybrids, as well as with the sample control for 24 h. The assay kit is then applied to the cells. The background is deduced and defined using the unstained cells.

Structural and Morphological Aspects

The cultured HEK293T and A549 cells which treated with the two different Cu nanodots/GA and Fe_3O_4 nanodots/GA hybrids with concentrations of 0.1 ng/µL and 100 ng/µL are microscopically investigated. A Nikon Eclipse Ts2 inverted microscope with a digital camera software (model Nikon DS-Ri2) is used to investigate and display images of the cells. All the cell samples are investigated, and the images are displayed after treatment with Cu nanodots/GA and Fe_3O_4 nanodots/GA hybrids for 24 h. Structural and morphological aspects are evaluated using NIS-Elements Software version 5.10.

Statistical Analysis

All experiments are independently repeated thrice. Statistical significance is set than 0.05. Student's *t*-test and analysis of variance (ANOVA) are used, as appropriate. GraphPad Prism version 5.03 is used for statistical analysis.

Results and Discussion

The morphologies of the prepared Cu and Fe_3O_4 nanodots/GA hybrids are shown in Figure 1. The results showed that the Cu nanodots had a 22—33 nm particle size with a quasi-spherical particle shape (Figure 1a). The histodiagram presented a normal distribution of the median particle size of 22 nm (Figure 1b), and more agglomeration is also detected. However, the Fe_3O_4 nanodots had a spherical particle size of 25—32 nm. The histogram shows a normal distribution, with a median particle size of 28 nm (Figure 1c and d). A homogeneous distribution of the synthesized nanodots stabilized by combination with GA is obtained and fewer agglomerations were observed. The reason for the difference in particle size between the Cu and Fe_3O_4 nanodots is the mode of interaction between the deposited Cu metal and the metal oxide (Fe_3O_4) nanodots with the GA polymer and the adopted chemical deposition preparation method.

EDX spectrum of the Cu nanodots/GA hybrids displayed high-intensity peaks of Cu at 1 keV and 8 keV (Figure 1e). These results agree well with those of previous studies on the synthesis of copper nanoparticles.[32–34] Approximately

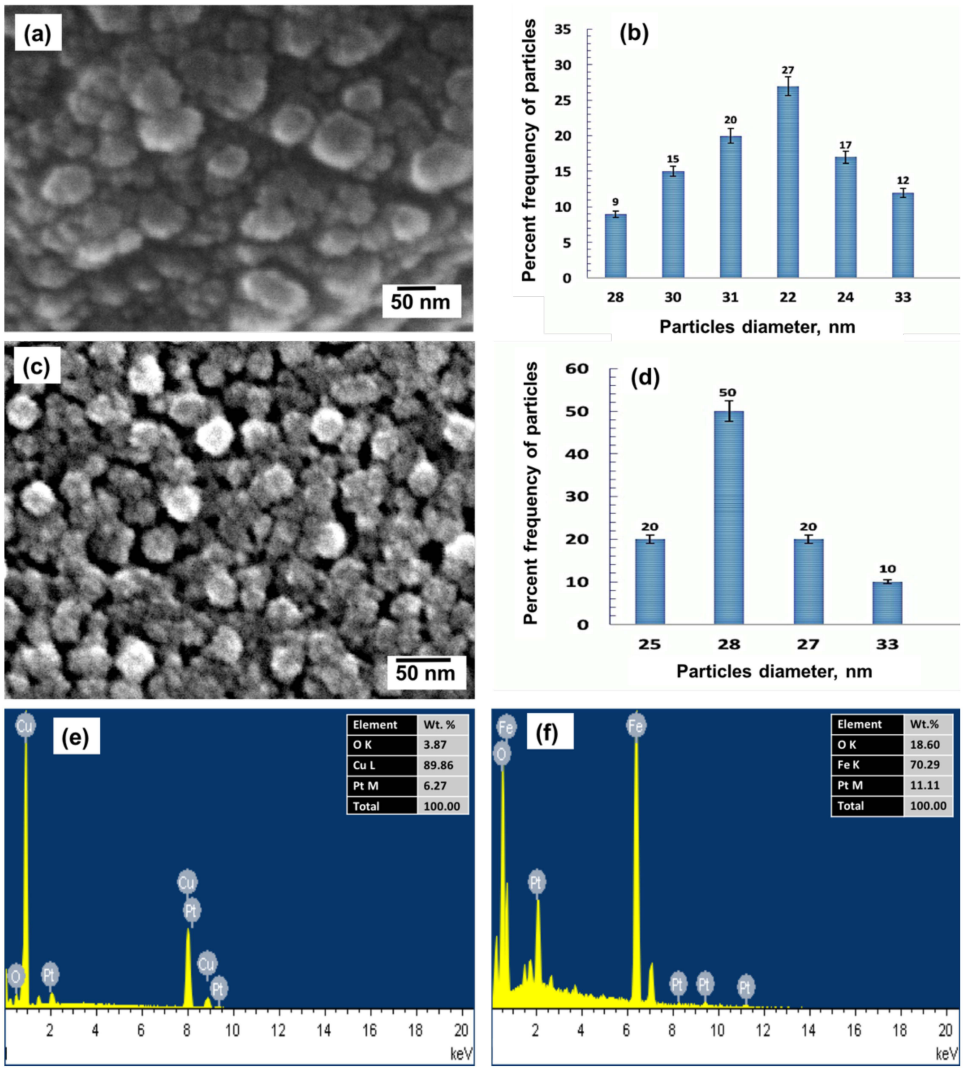

Figure 1 FE-SEM images, EDX compositional analysis and particle size distribution histodiagram of: (**a**, **b** and **e**) with copper nanodots/GA hybrid, (**c**, **d** and **f**) Fe_3O_4 nanodots/GA hybrid fabricated by chemical deposition method (platinum is the background of the coated layer by sputtering).

89.86% of the Cu is present in the prepared nanodots. The remaining 10.14% is oxygen and platinum, which is the background of the coated layer by sputtering during the preparation of the FE-SEM specimen for investigation. However, Fe_3O_4 nanodots/GA hybrids exhibit elemental iron at 0.5 keV and 6.5 keV with weight % is equal to 70.29%. (Figure 1f). The results agree with previous work reported in the literature.[35,36] It is also observed, the EDX spectrum is free of impurities confirming the high purity of the prepared Cu and Fe_3O_4 nanodots/GA hybrids.

TEM images at low and high magnifications are presented in Figure 2a and b, revealing that the Cu nanodots were monodisperse. This could be attributed to the electrostatic and steric interactions of GA as a capping agent with the Cu nanodots. It is also observed from the results that the Cu nanodots have a quasi spherical particle shape of particle size ranged 1.55–7.77 nm and the histodiagram present a normal distribution of median particle size of 3.5 nm (Figure 2c). HR-TEM images of the Fe_3O_4 nanodots prepared through chemical co-deposition are shown in Figure 2d and e. It was revealed that; The Fe_3O_4 nanodots dispersed in the GA stabilizing agent had a spherical shape with a particle size of 6.2—13.6 nm and the histogram presented a normal distribution of the median particle size 11.5 nm (Figure 2f). Clusters are also observed for the Fe_3O_4 nanodots/GA and Fe_3O_4 nanodots/GA hybrids. The formation of the clusters may be attributed to the high surface-area-to-volume ratio of the Cu and Fe_3O_4 nanodots which can be associated and dispersed in the GA capping agent.

GA is used as a capping agent for the in-situ stabilization of Cu and Fe_3O_4 nanodots by the formation of Cu/GA and Fe_3O_4/ GA hybrids. This process can facilitate the formation of a stable colloidal solution that can be used to detect

https://doi.org/10.2147/IJN.S498894

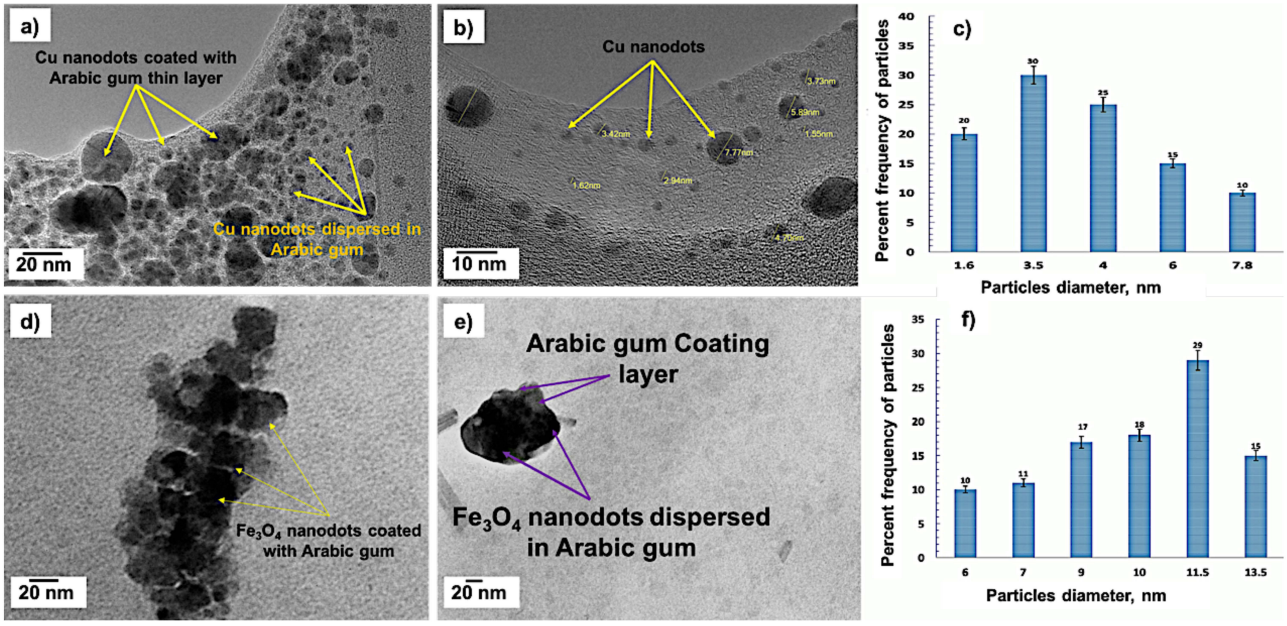

Figure 2 HR-TEM images and particle size distribution histodiagram of: (**a–c**) copper nanodots/GA hybrid, (**d–f**) Fe_3O_4 nanodots/GA hybrid fabricated by chemical deposition method.

cytotoxic effects on the cell lines under investigation. Figure 3a and b show the FT-IR spectra representing the different functional groups found in the Cu/ GA and Fe_3O_4/ GA hybrids. It is reported in the literature that; the Arabic gum mainly composed of carbohydrates and protein macromolecules, which have the ability to in-situ capping both Cu and Fe_3O_4 nanodots and inhibiting their aggregation in aqueous or polar solvents. The presence of Arabic gum functional groups enhanced its binding with the surface of Cu as well as the Fe_3O_4 nanodots,[37] and the FT-IR spectra of the Cu nanodots/ GA and Fe_3O_4/Arabic gum hybrids exhibited a wide band at 3400 cm^{-1}, indicating the existence of O-H…. O Intermolecular hydrogen bonding. The two bands observed at 2930 cm^{-1} and 2850 cm^{-1} are attributed to the vibrational modes of C-H in the aldehyde CHO group.[38] The band detected at 2340 cm^{-1} may be attributed to C ≡ O and/or C ≡ N groups. The band observed at 1630–1645 cm^{-1} corresponds to the characteristic amide (I) band, which is attributed to the vibration of C=O in the-$CONH_2$ group and the symmetric stretching of COO^- in carboxylic acid. The band observed at 1450–1300 cm^{-1} is associated with the quaternary amine -NH_3^+ groups and asymmetric stretching of the carboxylic COO^- as well as the vibrations of the–OH, –CH, and –COOH groups in uronic acid[39,40] The bands observed between 1150 and 700 cm^{-1} are attributed to the presence of the 1–4 linkage of galactose and 1–6 linkage of mannose, as well as the arabinogalactan carbohydrate residue of the GA capping agent.[41]

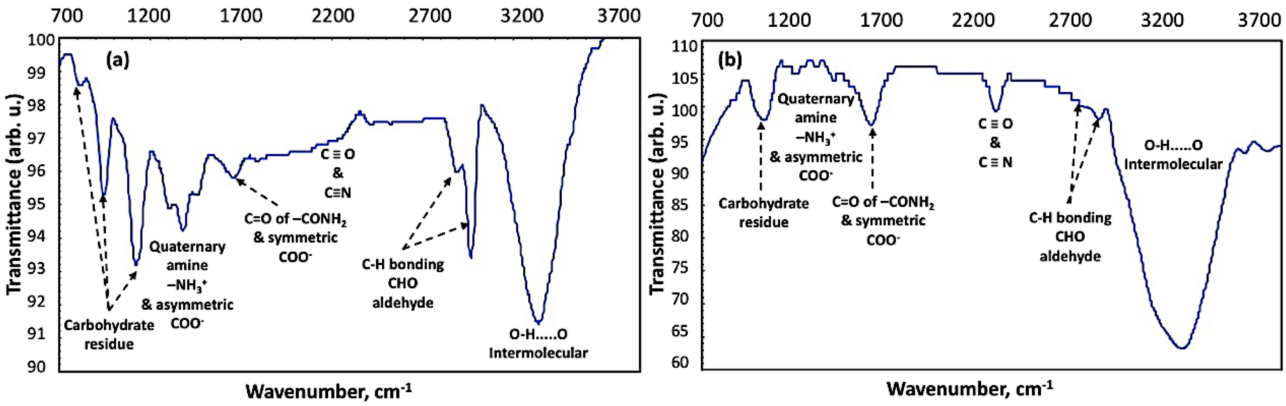

Figure 3 FT-IR charts of (**a**) Cu nanodots/ GA and (**b**) Fe_3O_4/GA hybrids synthesized by chemical deposition methods.

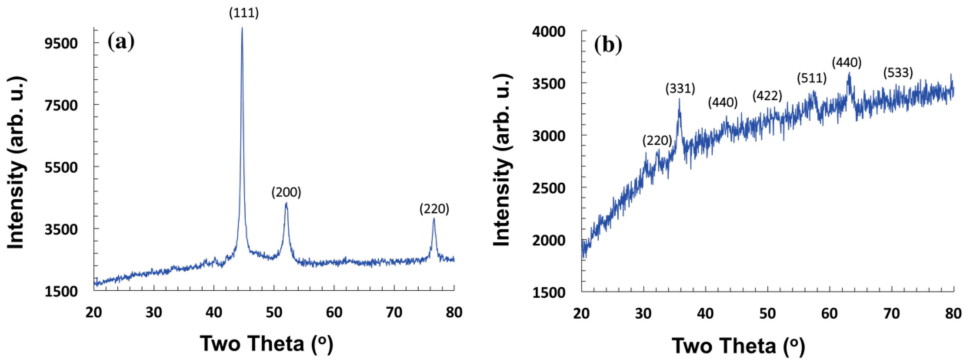

Figure 4 XRD patterns of: (**a**) copper nanodots and (**b**) Fe_3O_4 nanodots fabricated by chemical deposition method.

The XRD patterns of the synthesized copper and Fe_3O_4 nanodot/GA hybrids are shown in Figure 4. As shown in Figure 4a, the peaks observed at 2ɵ = 43°, 52°, and 78° correspond to (1 1 1), (2 0 0) and (2 2 0) representing a face-centered cubic structure of copper corresponding to the (JCPDS No. 85–1326) as reported in the literature.[42–44] The Scherrer crystallite size of the produced copper nanoparticles is calculated by the X-ray line broadening method using the mathematical formula of Scherrer's equation ($D = 0.9\ \lambda/B\ \cos\ \theta$) is estimated at 1.8×102 Å.[45]

The XRD pattern of the prepared Fe_3O_4 nanodots (Figure 4b) shows the XRD pattern of the synthesized Fe_3O_4 nanohybrid, with diffraction peaks at 2θ = 30.4°, 35.5°, 43.5°, 54°, 57.8°, 63°, and 74.8°, corresponding to the (220), (311), (400), (422), (511), (440), and (533) crystal planes of the Fe_3O_4 cubic crystal structure phase (JCPDS file no: 00–003-0863). These results suggest again the high purity of the prepared nanodots.[35,36] It is also revealed that gum arabic did not exhibit any additional peak. This is because of the low concentration of GA combined with Cu, as well as the Fe_3O_4 nanodots (1wt. %) which is beyond the detection limit of the XRD instrument.

GA can be considered as a nonmagnetic biopolymer material with no zero magnetic moment. However, they can exhibit some ferromagnetic properties owing to the combination of different magnetic nanoparticles, such as Fe_3O_4 nanoparticles. Figure 5 shows the magnetization/applied magnetic field (M/H) hysteresis loops of Fe_3O_4 nanodots. However, the Cu nanodots did not exhibit significant magnetic properties because of the non-magnetic character of the elemental Cu metal. This is because the copper atoms do not contain unpaired electrons. When a magnetic specimen is subjected to an external

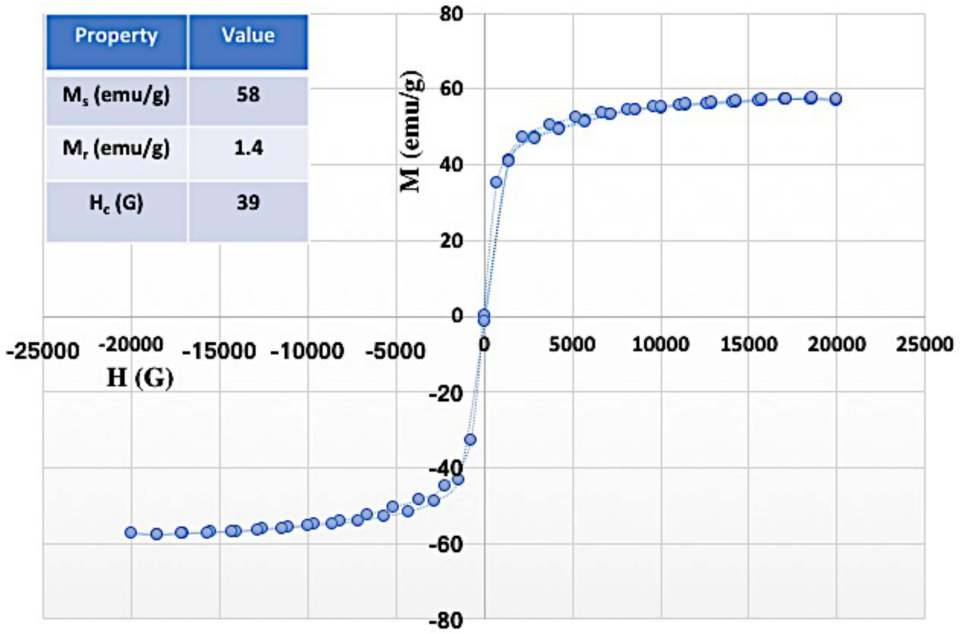

Figure 5 Magnetic hysteresis loop of the synthesized Fe_3O_4 nanodots by the chemical co-deposition method.

https://doi.org/10.2147/IJN.S498894

magnetic field of strength (H), the magnetization (M) hysteresis curve can be obtained by representing the correlation between M and H until the value of the magnetization reaches the saturation level, which called the M_s. The magnetization curve displays a hysteresis loop because not all domains return to their original alignment when H retches the saturation magnetization value. Thus, when the magnetic field H returns to zero, the M_r can be removed by applying a coercive field called H_c in the opposite direction. When the size of the material becomes nanoscale, the number of domains decreases, and a single domain can reach a critical particle size. Single-domain magnetic materials have a very narrow or no hysteresis loop and are said to be superparamagnetic materials.[17,46] The M_s, M_r, and H_c of the synthesized Fe_3O_4 nanodot/GA hybrid were measured under the effect of the 2-Tesla applied magnetic field at room temperature, as shown in Figure 5. The results showed that the M_s value of the synthesized Fe_3O_4 nanodot/ GA hybrid itself (57.8 emu/g). In addition, the Fe_3O_4 nanodots sample displayed M_s values lower than the bulk Fe_3O_4 value of 92 emu/g, as reported previously work of the literatures.[47] In addition, it has been reported in previous works[48,49] that several factors affect the M_s of Fe_3O_4 nanodots. The first factor is the entity of the spin-disorder layer, which increases with a decrease in the crystallite size of the Fe_3O_4 nanodots. The second factor can also be explained by the effect of the dipolar interactions between the Fe_3O_4 nanodots. The third factor is the particle shape of the Fe_3O_4 nanodots, which might influence the value of the saturation magnetization as a contribution from surface anisotropy. As the synthesized Fe_3O_4 nanoparticles were almost spherical in shape, zero contribution from surface anisotropy was expected. The further reduction in M_s can be attributed to the incomplete crystallization of Fe_3O_4 after the fast chemical co-deposition process. In addition, it was revealed from the results that a very narrow hysteresis loop for the samples was recorded and they exhibited small values of M_r and H_c. This indicates that the synthesized Fe_3O_4 nanodots readily display magnetization when subjected to an applied magnetic field with very small M_r and coercive force values. One possible mechanism for this unique form is the independent thermal fluctuation of small ferromagnetic domains inside the nanoparticles.[47] Our results are matched with previous work reported in the literature.[50] In this study, superparamagnetic iron oxide nanoparticles with a high saturation magnetization were synthesized in an air atmosphere. The magnetic results showed that the synthesis carried out according to the optimized conditions gave the highest M_s of 69.83 emu/g for the iron oxide nanoparticles synthesized under an air atmosphere. Magnetic measurements showed superparamagnetic behavior at room temperature for particle of the size 7.0±2.2 nm.[51] In another study, iron oxide nanoparticles were co-precipitated in air using different concentrations of sodium hydroxide (NaOH). Morphological observations showed that the size of the iron oxide nanoparticles was approximately 7.5 nm. The magnetization curves showed zero value of H_c, indicating that the samples are superparamagnetic, and the highest M_s (70.4 emu/g) is obtained at a stirring rate of 1100 rpm.[51] In addition, researchers have succeeded in synthesizing iron oxide nanoparticles from aqueous ferrous solutions in an air atmosphere by co-precipitation. The effect of the Fe^{2+}/Fe^{3+} ratio on the properties of the nanoparticles is investigated. The M_s of the nanoparticles increased from 37.6 emu/g 59.4 emu/g with an increase in the Fe^{2+}/Fe^{3+} ratio from 1/2 to 6/6, and the samples exhibited superparamagnetic properties with zero value of H_c. However, by increasing the ratio above 6/6, the samples started to show H_c values of 8 Oe, 22 Oe, and 33 Oe, and the Ms value increased to 74.3 emu/g.[52]

Cytotoxicity is detected at concentrations of 10–50 ng/μL of the produced Cu nanodots/GA and Fe_3O_4 nanodots/GA hybrids in A549 and HEK293T cell lines, respectively. The untreated control, Cu nanodots, and Fe_3O_4 nanodots hybrids combined with the GA control is not significantly different from each other. The results also revealed that the significance of Cu nanodots/arabic gum and Fe_3O_4 nanodots/ GA hybrid treatments had P value below 0.05. However, the prepared Fe_3O_4 nanodots/ GA hybrid did not show any significant effect on either A549 and HEK293T cell line because of its larger particle size than that of the Cu nanodots/ GA hybrid (Figure 2). Our results agree with previous work[53] which reported that; ultra-small Fe_3O_4 nanoparticles with particle size of 2.3—4.2 have lethal dosage of 100 mg/kg. In contrast, no obvious cytotoxicity was observed for the Fe_3O_4 nanoparticles with a size of 9.3 nm.

The results obtained from the MTT assay on A549 and HEK293T cells by applying different concentrations of copper nanodots/GA hybrid and Fe_3O_4 nanodot/GA hybrid showed different MTT values depending on the cell type. However, increasing the MTT concentration above a certain level accelerates any further increase in the optical density levels, regardless of cell number and rate of cell death, and does not allow cells to reduce MTT as much as they do at lower MTT concentrations. The MTT concentration reached its maximum at this point. An observation of decreasing or plateau formation in the optical density levels above the formazan produced before MTT-induced cell death should be selected as the optimum concentration and shown to vary depending on the MTT concentration for each typical cell type under investigation, cell number, and incubation

time.[54,55] Increased apoptosis is observed with the Cu nanodot-GA hybrid solution at concentrations as low as 0.1 ng/µL. Moreover, the measured preapoptosis of the treated A549 cells are 40% for 0.1 ng/µL, 91.4% for 1 ng/µL, 88% for 50 ng/ µL and 87.7% for 100 ng/µL respectively (Figure 6a). However, the treated HEK293T cells show preapoptosis of 89.9% for 0.1 ng/µL, 94.2% for 1 ng/µL, 76.2% for 50 ng/µL and 70.5% for 100 ng/µL respectively (Figure 6b).[56,57]

Apoptotic cells demonstrate morphological and biochemical characteristic features depending on the stimuli and cell type that can be observed during cellular death by flow and image cytometry. Translocation of phosphatidylserine from the inner side of the plasma membrane to the outer side of the cell surface is an early apoptotic event. Annexin V, which is a Ca^{2+}-dependent phospholipid-binding anticoagulant protein used as an early stage apoptotic indicator, has a high affinity for the phosphatidylserine membrane, and fluorochrome-labeled Annexin V can be used to detect the exposed phosphatidylserine membrane on the outside cell surface using flow cytometry. Translocation of the Phosphatidylserine membrane indicates loss of membrane integrity, which is accompanied by later stages of cell death resulting from either apoptotic or necrotic processes. Therefore, staining with Annexin V in conjunction with propidium iodide was used to identify early and late apoptotic cells.[58–64] Propidium iodide was used as a red fluorescent nuclear and chromosomal counterstaining dye. Viable cells that have healthy cell membranes with intact membranes exclude propidium iodide,

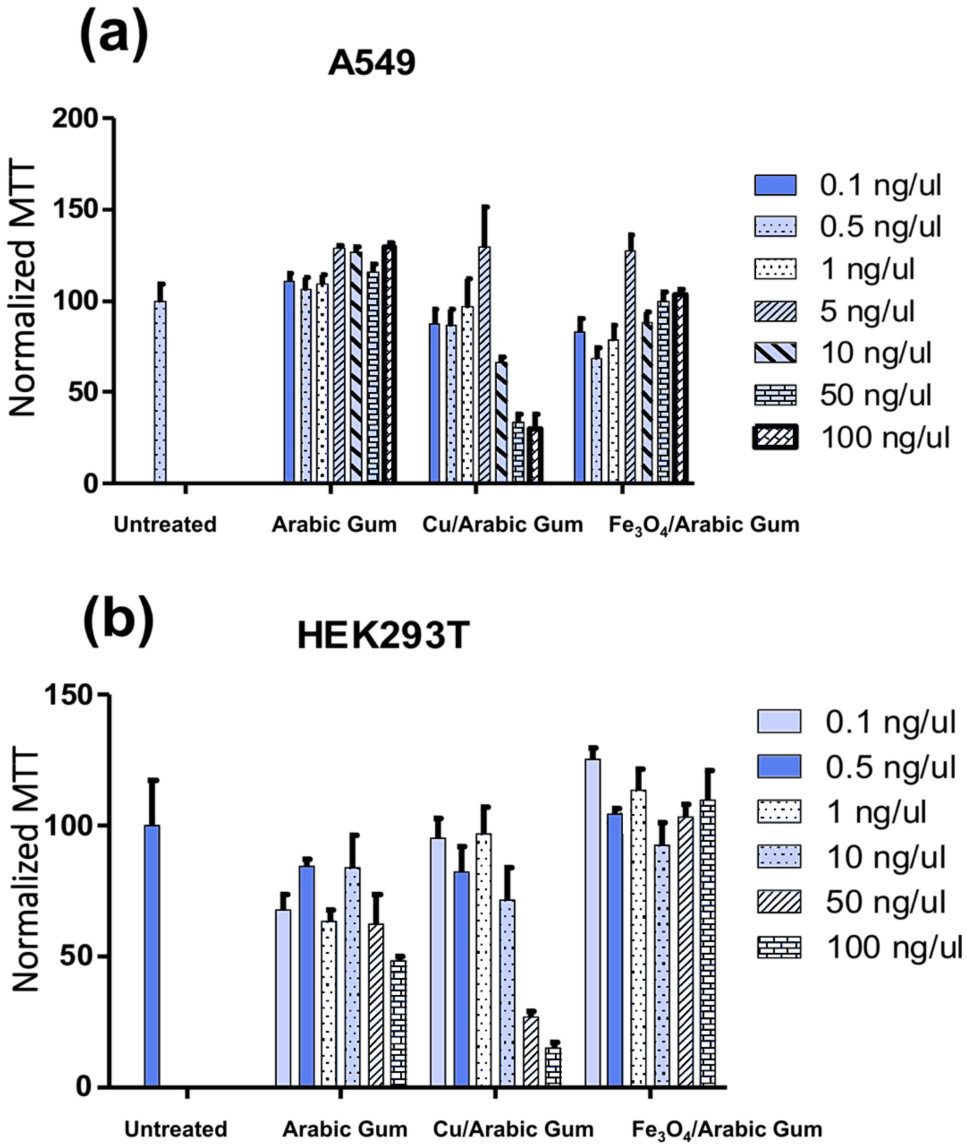

Figure 6 Cell viability assay showing changes with treatment with the Cu and Fe_3O_4 nanodots/GA hybrids studied samples at various concentration: (**a**), A549 and (**b**) HEK 293T.

https://doi.org/10.2147/IJN.S498894

whereas the disturbed membranes of dead and damaged cells are permeable to propidium iodide. Therefore, cells that are considered viable are both annexin V-negative (-) and propidium iodide-negative (-), while cells that are in early apoptosis are Annexin V (+) and propidium iodide (-), and cells that are in late apoptosis or already dead are both Annexin V (+) and propidium iodide (+).[51–57] Flow cytometry is used to identify the number of apoptotic and non-apoptotic cells. Figures 7 and 8 show the typical forward scattering (FSC-A) of Annexin V against the side scattering (SSC-A) of propidium iodide dot plots of A549 and Hek293T under the effect of copper/GA hybrid nanodots. Quadrants

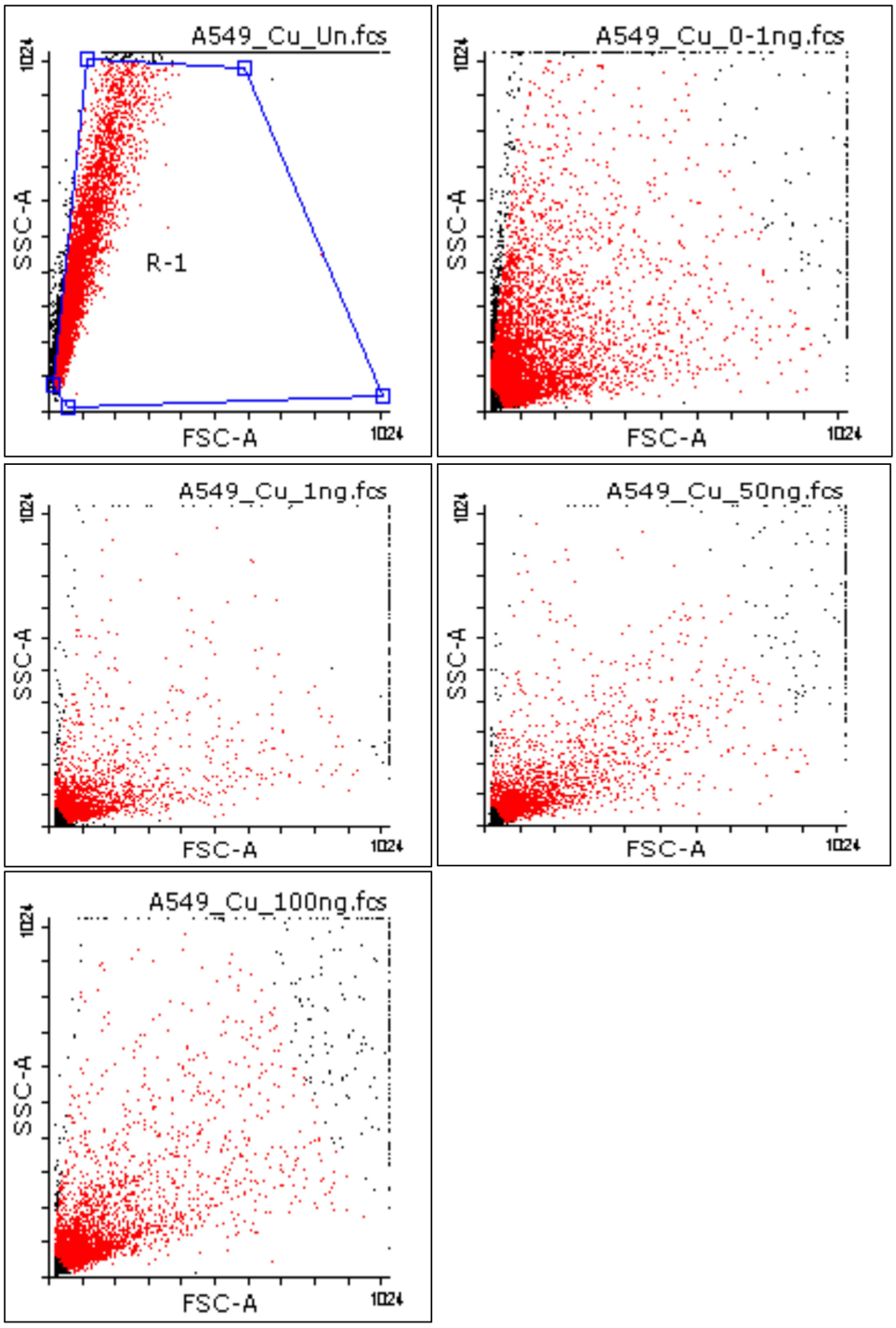

Figure 7 Flow cytometry showing the effect of treatment Cu nanodots/ GA hybrids with different concentrations on the pre-apoptotic marker (Annexin V/ Propidium iodide) (A549 cell line).

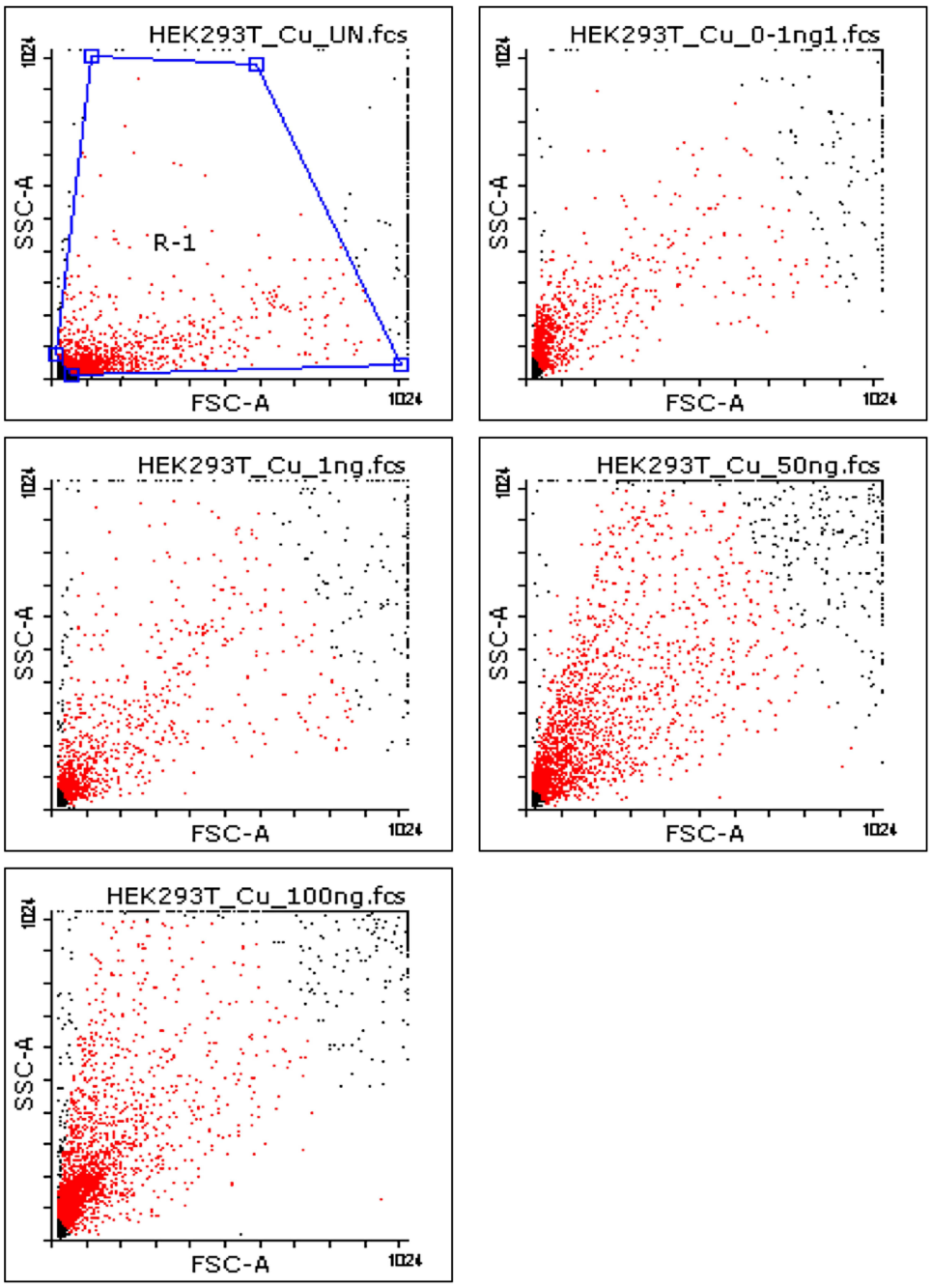

Figure 8 Flow cytometry showing the effect of treatment Cu nanodots/GA hybrids with different concentrations on the pre-apoptotic marker (Annexin V/ Propidium iodide) (HEK 293T cell line).

are set to identify the maximum fluorescence intensity for background staining with Annexin V. Test samples with higher levels of Annexin V binding were considered positive and apoptotic. It is revealed from the obtained results that; the binding with the Annexin V which correspond with the treatment cells A549 and Hek293T by copper/ GA hybrids nanodots. However, the Fe_3O_4/ GA hybrids showed no significant effects. It was clear from the results that when apoptosis occurs by the effect of the extrinsic pathway with the effect of Cu nanodots/GA hybrids on the A549 and Hek293T cancer cells, translocation of the phosphatidylserine membrane from the inner side of the plasma membrane to the outer side of the cell surface occurs, which can be combined with Annexin V and blinded to Propidium iodide.[58–64]

https://doi.org/10.2147/IJN.S498894

The results revealed that after incubating the treated A549 cells with 0.1 ng/μL of the Cu nanodots/ GA hybrid, they appeared healthy with minor cellular debris. However, after incubating the treated HEK293T cells with 0.1 ng/ μL of the Cu nanodots/ GA hybrid, they looked less healthy than usual with a large amount of cellular debris. However, after treatment, both cell lines treated with 100 ng/μL of Cu nanodots/ GA hybrid, both A549 and HEK293T, had many cell deaths and reformed Cu nanoparticle crystals (see Figure 9). The reason behind that; the Cu nanodots can release Cu ions (Cu^{2+} and Cu^{+}) during the incubation time and may interact with DNA molecules and insert between the nucleic acid strands and disrupting the different biochemical and metabolic processes. The mixed valent Cu ions (Cu^{2+} and Cu^{+}) can produce reactive oxygen species and independently induce the generation of hydroxyl radicals, inducing oxidative stress, damaging DNA, and causing cell cycle arrest. Also, it is expected that, the combined GA with the Cu nanodots activates and promotes redox reactions between the released Cu^{2+} and Cu^{+}, resulting in the depletion of deoxyribonucleotides, DNA synthesis inhibition, and G_1 phase cell cycle arrest, ultimately triggering apoptosis. Also by activating various signaling pathways, such as the mitogen-activated protein kinase and c-Jun N-terminal kinase pathways. Simultaneously, in mitochondria, Cu ions can induce the Fenton reaction with endogenous H_2O_2, generating highly reactive $^{\bullet}OH$ radicals that form oxidative stress as well as can cause mitochondrial membrane depolarization, cell cycle arrest, and the induction of apoptosis.[65–68]

Collectively, our findings provide and suggest powerful evidence of new perspective for the therapeutic approaches of the cytotoxicity of metallic nanoparticles against cancer cells. To the best of our knowledge, the current study is the first work that report the combination of Cu and Fe_3O_4 nanodots with GA to produce new hybrid materials and performed its biological activity on the A549 lung cancer and human embryonic kidney (HEK239T) cells lines. Although, Cu nanodots/GA are found to have significant cytotoxic activity on the A549 lung cancer and human embryonic Kidney

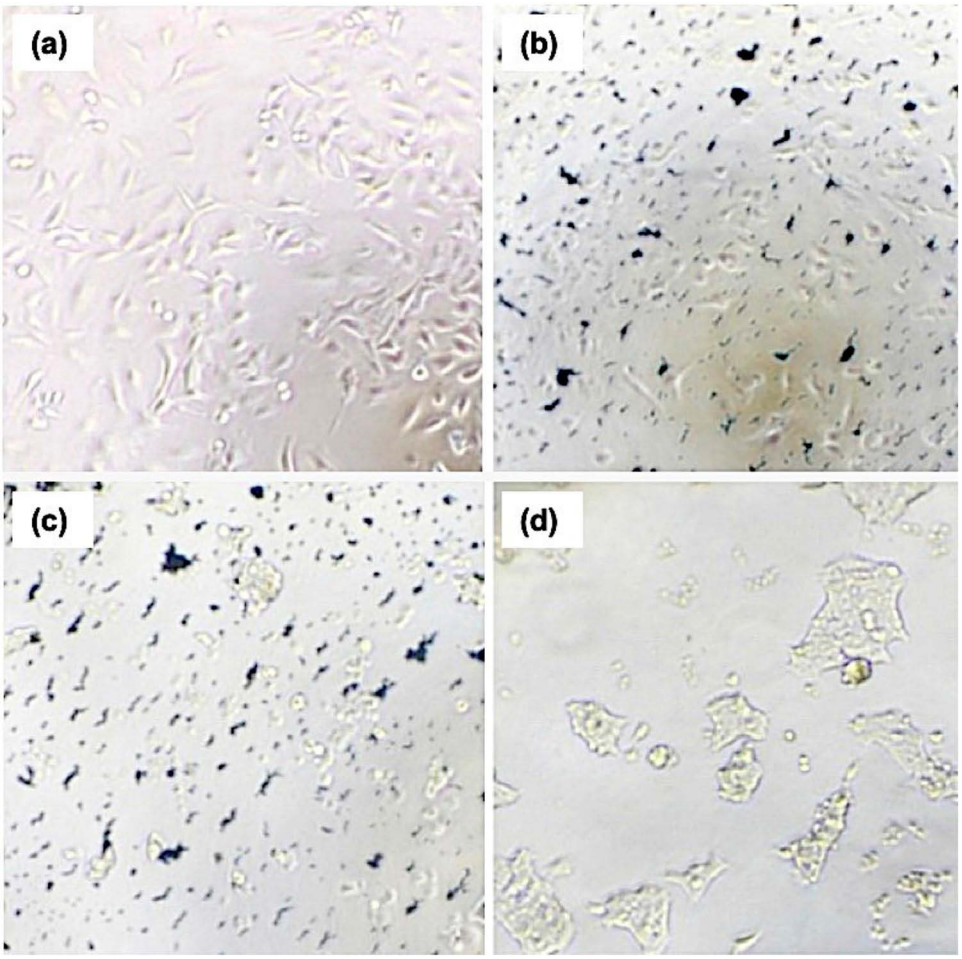

Figure 9 Images analysis of the morphological changes: (**a**) A549: 0.1 ng/μL Cu. Conc., (**b**) A549: 100 ng/μL of Cu nanodots/ GA hybrids concentration, (**c**) HEK293T: 0.1 ng/μL Cu nanodots conc., and (**d**) HEK293T: 100 ng/μL of Cu nanodots/ GA hybrids concentration.

(HEK239T) cells lines however, Fe_3O_4 nanodots/ GA hybrids did not show any significant cytotoxic activity. From this investigation, it is concluded that the synthesized Cu nanodots/GA hybrid can be used as anticancer agents. It can also be used to address a number of challenges in the field of nanomedicine and can find immense application as anticancer agent in the consumer and industrial products.

Conclusion

Cu and Fe_3O_4 nanodots combined with GA biopolymers are synthesized using chemical reduction and co-precipitation methods, respectively. The GA hybrid with Cu nanodots displayed a face-centered cubic structure and did not exhibit significant magnetic properties owing to their non-magnetic behaviour. However, the Fe_3O_4 nanodots/ GA hybrid has spinel structure and exhibited unique magnetic properties. The use of GA as a capping agent to stabilize the produced Cu in situ, as well as Fe_3O_4 nanodots, is considered a low-cost and simple method to disperse these nanodots in aqueous solutions for further diagnosis and treatment applications in cancer cells. The MTT and the flow cytometry assays of the produced Cu nanodots/ GA hybrid showed a strong reduction in the viability of both A549 and HEK239T cells at 50 and 100 ng/μL. However, the prepared Fe_3O_4 nanodots/ GA hybrid does not show any significant effect owing to its larger particle size than that of the Cu nanodots/ GA hybrid. The mode of cell death of the treated A549 and HEK293T cell lines by the Cu nanodots/ GA hybrid is monitored by the Preapoptosis assay. Also, after treatment of the investigated cell lines with the Cu nanodots/ GA hybrid, both A549 and HEK293T have a lot of dead cells and reformed nanoparticles crystals dispersed within the cell contents.

Acknowledgments

The author extends the appreciation to the Deanship of Postgraduate Studies and Scientific Research at Majmaah University for funding this research work through the project number (R-2025-1552).

Author Contributions

All authors made a significant contribution to the work reported, whether that is in the conception, study design, execution, acquisition of data, analysis and interpretation, or in all these areas; took part in drafting, revising or critically reviewing the article; gave final approval of the version to be published; have agreed on the journal to which the article has been submitted; and agree to be accountable for all aspects of the work.

Disclosure

The authors report no conflicts of interest in this work.

References

1. Zhai D, Zhang T, Guo J, Fang X, Wei J. Water-based ultraviolet curable conductive inkjet ink containing silver nano-colloids for flexible electronics. *Colloids Suf A*. 2013;424:1. doi:10.1016/j.colsurfa.2013.01.055
2. Dong C, Cai H, Zhang X, Cao C. Synthesis and characterization of monodisperse copper nanoparticles using gum acacia. *Physica E*. 2014;57:12–20. doi:10.1016/j.physe.2013.10.025
3. Wen J, Li J, Liu S, Chen Q-Y. Preparation of copper nanoparticles in a water/oleic acid mixed solvent via two-step reduction method. *Colloids Suf A*. 2011;373:29–35. doi:10.1016/j.colsurfa.2010.10.009
4. Kumar RV, Mastai Y, Diamant Y, Gedanken A. Sonochemical synthesis of amorphous Cu and nanocrystalline Cu2O embedded in a polyaniline matrix. *J Mater Chem*. 2001;11:1209. doi:10.1039/b005769j
5. Kitchens CL, Roberts CB. Copper nanoparticle synthesis in compressed liquid and supercritical fluid reverse micelle systems. *Ind Eng Chem Res*. 2004;43:6070. doi:10.1021/ie0497644
6. Remita S, Mostafavi M, Delcourt MO. Bimetallic AgPt and AuPt aggregates synthesized by radiolysis. *Radiat Phys Chem*. 1996;47:275. doi:10.1016/0969-806X(94)00172-G
7. Vitulli G, Bernini M. Bertozzi S, et al. Nanoscale copper particles derived from solvated Cu atoms in the activation of molecular oxygen. *Chem Mater*. 2002;14:1183. doi:10.1021/cm011199x
8. Dey GR. Reduction of the copper ion to its metal and clusters in alcoholic media: a radiation chemical study. *Radiat Phys Chem*. 2005;74:172–184. doi:10.1016/j.radphyschem.2005.04.012
9. Park BK, Jeong S, Kim D, Moona J, Limb S, Kim JS. Synthesis and size control of monodisperse copper nanoparticles by polyol method. *J Colloid Interface Sci*. 2007;311:417. doi:10.1016/j.jcis.2007.03.039
10. Dhas NA, Raj CP, Gedanken A. Synthesis, characterization, and properties of metallic copper nanoparticles. *Chem Mater*. 1998;10:1446. doi:10.1021/cm9708269

11. Pham LQ, Sohn JH, Kim CW. Copper nanoparticles incorporated with conducting polymer: effects of copper concentration and surfactants on the stability and conductivity. *Colloid Interface Sci*. 2012;365(1):103. doi:10.1016/j.jcis.2011.09.041
12. Abdulla-Al-Mamun M, Kusumoto Y, Muruganandham M. Simple new synthesis of copper nanoparticles in water/acetonitrile mixed solvent and their characterization. *Mater Lett*. 2009;63:2007–2009. doi:10.1016/j.matlet.2009.06.037
13. Kobayashi Y, Shirochi T, Yasuda Y, Morita T. Preparation of metallic copper nanoparticles in aqueous solution and their bonding properties. *Solid State Sci*. 2011;13:553. doi:10.1016/j.solidstatesciences.2010.12.025
14. Vaseem M, Lee KM, Kim DY, Hahh YB. Parametric study of cost-effective synthesis of crystalline copper nanoparticles and their crystallographic characterization. *Mater Chem Phys*. 2011;125:334. doi:10.1016/j.matchemphys.2010.11.007
15. Lai D, Liu T, Jiang G, Chen W. Synthesis of highly stable dispersions of copper nanoparticles using sodium hypophosphite. *J Appl Polym Sci*. 2013;128:1443. doi:10.1002/app.38109
16. Răcuciu M, Barbu-Tudoran L, Oancea S. Aspartic acid stabilized iron oxide nanoparticles for biomedical applications. *Nanomate*. 2022;12:1151. doi:10.3390/nano12071151
17. Daoush WM. Co-precipitation and magnetic properties of magnetite nanoparticles for potential biomedical applications. *J Nanomed Res*. 2017;5:1–5.
18. Özel F, Karaagac O, Tokay E, Köçkar F, Köçkar H. A simple way to synthesize tartaric acid, ascorbic acid and their mixture coated superparamagnetic iron oxide nanoparticles with high saturation magnetisation and high stability against oxidation: characterizations and their biocompatibility studies. *J Magn Magn Mate*. 2019;474:Pages654–660. doi:10.1016/j.jmmm.2018.11.025
19. Ozel F, Kockar H, Karaagac O. Growth of iron oxide nanoparticles by hydrothermal process: effect of reaction parameters on the nanoparticle size. *J Supercond Nov Magn*. 2015;28:823–829. doi:10.1007/s10948-014-2707-9
20. Ozel F, Kockar H. A simple method of synthesis and characterizations of oleate-coated iron oxide nanoparticles. *J Supercond Nov Magn*. 2017;30:2023–2027. doi:10.1007/s10948-016-3844-0
21. Karaagac O, Kockar H, Beyaz S, Tanrisever T. A simple way to synthesize superparamagnetic iron oxide nanoparticles in air atmosphere: iron ion concentration effect. *IEEE Trans Magn*. 2010;46(12):3978–3983. doi:10.1109/TMAG.2010.2076824
22. Zhang D, Yang H, Chen Q. Gelatin-stabilized copper nanoparticles: synthesis, morphology, and their surface-enhanced Raman scattering properties. *Physica B*. 2013;415:44. doi:10.1016/j.physb.2013.01.041
23. Rao YN, Banerjee D, Datta A, Das SK, Guin R, Saha A. Gamma irradiation route to synthesis of highly re-dispersible natural polymer capped silver nanoparticles. *Radiat Phys Chem*. 2010;79:1240. doi:10.1016/j.radphyschem.2010.07.004
24. Abubakar A. *Gum Arabic, Report on Survey of Selected Agricultural Raw Materials in Nigeria*. Kano, Nigeria; 2004.
25. Chandraju S, Mythily R, Chidan CS. Isolation of simple sugar from a hydro colloid: gum Arabic. *IJLRST*. 2012;4(11):34–36.
26. Suárez-Cerda J, Espinoza-Gómez H, Alonso-Núñez G, Rivero IA, Gochi-Ponce Y, Flores-López LZ. A green synthesis of copper nanoparticles using native cyclodextrins as stabilizing agents. *J Saudi Chem Society*. 2017;21:341–348. doi:10.1016/j.jscs.2016.10.005
27. El-Batal AI, Al-Hazmi NE, Mosallam FM, El-Sayyad GS. S.El -Sayyad. Biogenic synthesis of copper nanoparticles by natural polysaccharides and *Pleurotus ostreatus* fermented fenugreek using gamma rays with antioxidant and antimicrobial potential towards some wound pathogens. *Microb Pathog*. 2018;118:159–169. doi:10.1016/j.micpath.2018.03.013
28. Chawla P, Kumar N, Bains A. Sneh Punia. Gum arabic capped copper nanoparticles: synthesis, characterization, and applications.*Int J Biol Macromol*. 2020;146:232–242. doi:10.1016/j.ijbiomac.2019.12.260
29. Abdel Halim AS, Ali MA, Inam F, Alhalwan AM, Daoush WM. Fe3O4-coated CNTs-gum arabic nano-hybrid composites exhibit enhanced anti-leukemia potency against AML cells via ROS-mediated signaling. *Int J Nanomedicine*. 2024;19:7323–7352. doi:10.2147/IJN.S467733
30. Sultan SA, Khawaji MH. Alsughayyir J, Alfhili MA, Alamri HS, Alrfaei BM. Antileukemic activity of sulfoxide nutraceutical allicin against THP-1 cells is associated with premature phosphatidylserine exposure in human erythrocytes. *Saudi J Biol Sci*. 2020;27:3376–3384. doi:10.1016/j.sjbs.2020.09.005
31. Alghamdi A, Aldossary W, Albahkali S, Alotaibi B, Alrfaei BM. The loss of microglia activities facilitates glaucoma progression in association with CYP1B1 gene mutation (p. Gly61Glu. *PLoS One*. 2020;15:e0241902. doi:10.1371/journal.pone.0241902
32. Ebrahimi K, Shiravand S, Mahmouvand H. Biosynthesis of copper nanoparticles using aqueous extract of Capparis spinosa fruit and investigation of its antibacterial activity. *M Pharma J*. 2017;21:866–871.
33. Cerchier P, Dabala M, Brunelli K. Green synthesis of copper nanoparticles with ultrasound assistance. *Green Process Synth*. 2017;6:311–316.
34. Sebeia N, Jabli M, Ghith A, Saleh TA. Eco-friendly synthesis of Cynomorium coccineum extract for controlled production of copper nanoparticles for sorption of methylene blue dye. *Arab J Chem*. 2020;13:4263–4274. doi:10.1016/j.arabjc.2019.07.007
35. Aghazadeh M, Karimzadeh I, Ghannadi Maragheh M, Reza Ganjali M. Enhancing the supercapacitive and superparamagnetic performances of iron oxide nanoparticles through yttrium cations electro-chemical doping. *Mater Res*. 2018;21:1–10. doi:10.1590/1980-5373-mr-2018-0094
36. Gupta H, Kumar R, Park HS, Jeon BH. Photocatalytic efficiency of iron oxide nanoparticles for the degradation of priority pollutant anthracene. *Geosystem Eng*. 2016;1:21–27.
37. Al-zharani M, Alyami NM, Qurtam AA, et al. Use of multi-walled carbon nanotubes (MWCNTs) stabilized in Arabic gum colloidal solution to induce genotoxicity and apoptosis of human breast and lung cancer cell lines. *Front Mater*. 2023;10:1229637.
38. Bashir M, Haripriya S. Assessment of physical and structural characteristics of almond gum. *Int J Biol Macromol*. 2016;93:476–482. doi:10.1016/j.ijbiomac.2016.09.009
39. Grant J, Cho J, Allen C. Self-assembly and physicochemical and rheological properties of a polysaccharide-surfactant system formed from the cationic biopolymer chitosan and nonionic sorbitan esters. *Langmuir*. 2006;22:4327–4335. doi:10.1021/la060017g
40. Qian F, Cui F, Ding J, Tang C, Yin C. Chitosan graft copolymer nanoparticles for oral protein drug delivery: preparation and characterization. *J Biol Macromol*. 2006;7:2722.
41. Rezaei A, Nasirpour A, Tavanai H. Fractionation and some physicochemical properties of almond gum (Amygdalus communis L.) exudates. *Food Hydrocoll*. 2016;60:461–469. doi:10.1016/j.foodhyd.2016.04.027
42. Yallappa S, Manjanna J, Sindhe MA, Satyanarayan ND, Pramod SN, Nagaraja K. Microwave assisted rapid synthesis and biological evaluation of stable copper nanoparticles using T. arjuna bark extract. *Spectrochim Acta Part A*. 2013;110:108–115. doi:10.1016/j.saa.2013.03.005
43. Harne S, Sharma A, Dhaygude M, Joglekar S, Kodam K, Hudlikar M. Novel route for rapid biosynthesis of copper nanoparticles using aqueous extract of Calotropis procera L. latex and their cytotoxicity on tumor cells. *Colloids Surf B*. 2012;95:284–288. doi:10.1016/j.colsurfb.2012.03.005

44. Taghizadeh F. The study of structural and magnetic properties of NiO nanoparticles. *Opt Photonics J*. 2016;6:164–169. doi:10.4236/opj.2016.68B027
45. Daoush WM, Alkhuraiji TS, Khamis MA, et al. Microstructure and electrical properties of carbon short fiber reinforced copper composites fabricated by electroless deposition followed by powder metallurgy process. *Carbon Lett*. 2020;30:247–258. doi:10.1007/s42823-019-00093-1
46. Hossam H. Walid Daoush "Preparation of 2-5 µm magnetite powder from high carbon ferrochrome (Fe-Cr) Alloy", 23rd International Conference on Metallurgy and Materials, METAL 2014; May 21-23, 2014; Brno, Czech Republic.
47. Cornell RM, Schwertmann U. *The Iron Oxides: Structure, Properties, Reactions, Occurrences and Uses. (2nd Edn)*. Germany: Wiley VCH Weinheim; 2004.
48. Wang B, Wei Q, Qu S. Synthesis and characterization of uniform and crystalline magnetite nanoparticles via oxidation-precipitation and modified co-precipitation methods. *Int J Electrochem Sci*. 2013;8(2013):3786–3793. doi:10.1016/S1452-3981(23)14431-2
49. Goya GF. Gerardo F Goya Magnetic dynamics of $Zn_{57}Fe_2O_4$ nanoparticles dispersed in a ZnO matrix. *IEEE Trans Magn*. 2002;38(5):2610–2612. doi:10.1109/TMAG.2002.803204
50. Karaagac O, Kockar H. A simple way to obtain high saturation magnetization for superparamagnetic iron oxide nanoparticles synthesized in air atmosphere: optimization by experimental design. *J Magn and Magn Mate*. 2016;409:Pages116–123. doi:10.1016/j.jmmm.2016.02.076
51. Karaagac O, Kockar H. Effect of synthesis parameters on the properties of superparamagnetic iron oxide nanoparticles. *J Supercond Nov Magn*. 2012;25:2777–2781. doi:10.1007/s10948-011-1264-8
52. Karaagac O, Kockar H. Iron oxide nanoparticles co-precipitated in air environment: effect of $[Fe^{+2}]/[Fe^{+3}]$ ratio. *IEEE Trans Magn*. 2012;48(4):1532–1536. doi:10.1109/TMAG.2011.2173313
53. Wu L, Wen W, Wang X, et al. Ultrasmall iron oxide nanoparticles cause significant toxicity by specifically inducing acute oxidative stress to multiple organs. *Part Fiber Toxicol*. 2022;19:24. doi:10.1186/s12989-022-00465-y
54. Carreño E, Alberto A, de Souza C, de Mello H, Henriques-Pons A, Alves LA. Considerations and technical pitfalls in the employment of the MTT assay to evaluate photosensitizers for photodynamic therapy. *Appl Sci*. 2021;11:2603. doi:10.3390/app11062603
55. Plumb J, Milroy R, Kaye SB. Effects of the pH dependence of 3-(4,5-dimethylthiazol-2-yl)-2,5-diphenyl-tetrazolium bromide- formazan absorption on chemosensitivity determined by a novel tetrazolium-based assay. *Cancer Res*. 1989;49:4435–4440.
56. Yusefi M, Shameli K, Ali RR, Pang S-W, Teow S-Y. Evaluating anticancer activity of plant-mediated synthesized iron oxide nanoparticles using *Punica granatum* fruit peel extract. *J Mol Struct*. 2020;1204:127539. doi:10.1016/j.molstruc.2019.127539
57. Izadiyan Z, Shameli K, Miyake M, et al. Cytotoxicity assay of plant-mediated synthesized iron oxide nanoparticles using Juglans regia green husk extract. *Arab J Chem*. 2018.
58. Bourebaba L, Michalak I, Röcken M, Marycz K. Cladophora glomerata methanolic extract decreases oxidative stress and improves viability and mitochondrial potential in equine adipose derived mesenchymal stem cells (ASCs. *Biomed Pharm*. 2019;111:Pages6–18. doi:10.1016/j.biopha.2018.12.020
59. Anthony RS, McKelvie ND, Cunningham AJ, Craig JI, Rogers SY, Parker AC. Flow cytometry using annexin V can detect early apoptosis in peripheral blood stem cell harvests from patients with leukaemia and lymphoma. *BMT*. 1998;21(5):441–446.
60. Vermes I, Haanen C, Steffens-Nakken H, Reutelingsperger CP. A novel assay for apoptosis. Flow cytometric detection of phosphatidylserine expression on early apoptotic cells using fluorescein labelled annexin V. *J Immunol Methods*. 1995;184:39–51. doi:10.1016/0022-1759(95)00072-I
61. Casciola-Rosen L, Rosen A, Petri M, Schlissel M. Surface blebs on apoptotic cells are sites of enhanced procoagulant activity: implications for coagulation events and antigenic spread in systemic lupus erythematosus. *Proc Nat Acad Sci USA*. 1996;93:1624–1629. doi:10.1073/pnas.93.4.1624
62. van Engeland M, Ramaekers FC, Schutte B, Reutelingsperger CP. A novel assay to measure loss of plasma membrane asymmetry during apoptosis of adherent cells in culture. *Cytometry*. 1996;24:131–139. doi:10.1002/(SICI)1097-0320(19960601)24:2<131::AID-CYTO5>3.0.CO;2-M
63. Wlodkowic D, Skommer J, Darzynkiewicz Z. SYTO probes in the cytom- etry of tumor cell death. *Cytometry A*. 2008;73:496–507. doi:10.1002/cyto.a.20535
64. Telford WG, Komoriya A, Packard BZ. Multiparametric analysis of apoptosis by flow and image cytometry. *Meth- Ods Mol Biol*. 2004;263:141–160.
65. Denoyer D, Masaldan S, Fontaine SL, Cater MA. Targeting copper in cancer therapy: 'Copper that cancer'. *Metallomics Integrated Biometal Sci*. 2015;7(11):1459–1476. doi:10.1039/C5MT00149H
66. Shimada K, Reznik E, Stokes ME, et al. Copper-binding small molecule induces oxidative stress and cell-cycle arrest in glioblastoma-patient-derived cells. *Cell Chem Biol*. 2018;25(5):585–94.e7. doi:10.1016/j.chembiol.2018.02.010
67. Tsai CY, Finley JC, Ali SS, Patel HH, Howell SB. Copper influx transporter 1 is required for FGF, PDGF and EGF-induced MAPK signaling. *Biochem Pharmacol*. 2012;84(8):1007–1013. doi:10.1016/j.bcp.2012.07.014
68. Wu H, Guo H, Liu H, et al. Copper sulfate-induced endoplasmic reticulum stress promotes hepatic apoptosis by activating chop, jnk and caspase-12 signaling pathways. *Ecotoxicol Environ Saf*. 2020;191:110236. doi:10.1016/j.ecoenv.2020.110236